Ocean and Coastal Research

Case Report
Special Article Collection
Di Domenico, M.; Andriguetto-Filho, J.M. and Lopes, R.M. (Eds)
An ocean of science, worms, and humaneness:
a tribute to Paulo Lana
http://doi.org/10.1590/2675-2824072.23095
ISSN 2675-2824

Direct hydrodynamic measurements at the upper shoreface of a sandy beach in Paraná - Brazil

Mauricio A. Noernberg[1*], Pedro A. Rodrido[2]

[1] Center for Marine Studies – Federal University of Paraná (P.O. Box 61 – 83255-976 – Pontal do Paraná – PR – Brazil).
[2] Ocean and Coastal Systems Graduate Program – Federal University of Paraná (P.O. Box 61 – 83255-976 – Pontal do Paraná – PR – Brazil).

* Corresponding author: m.noernberg@ufpr.br

Abstract

Sandy shorelines show heightened susceptibility to alterations, highlighting the importance of reliable field measurements in forecasting coastal evolution. This study offers direct hydrodynamic measurements from the upper shoreface of a sandy beach in Paraná. We observed five distinct oceanographic conditions, including a high-energy event. Notably, wave height showed a positive correlation with northward longshore currents. During pre- and post-frontal periods, cross-shore flow predominates over longshore currents, particularly evident during low tides with pronounced offshore flow. These findings provide valuable insights for researchers seeking to quantify and model longshore sediment transport dynamics and morphological changes along sandy coastlines.

Keywords: Longshore current, Cross-shore current, Sediment transport, Coastline

INTRODUCTION

The coastal zone is a dynamic environment shaped by intricate interactions among land, sea, and atmospheric forces and stands as one of the most densely populated and extensively developed regions on the planet. Sandy shorelines, comprising 31% of ice-free coastlines globally, are particularly susceptible to change. According to Luijendijk et al. (2018), approximately 24% of the sandy beaches worldwide are eroding at rates exceeding 0.5 m yr^{-1}, whereas 28% are accreting and 48% remain stable. The potential impact of climate-induced sea-level rise on sandy beach erosion, excluding nourishment efforts, could lead to a global land loss of 6000–17,000 km^2 during the 21st century, potentially displacing 1.6–5.3 million individuals (Hinkel et al., 2013).

The access to the shoreface poses significant challenges, with scientific and engineering efforts prioritizing the surf zone, beach face (swash zone), and landward areas, thus neglecting direct measurements (Hamon-Kerivel, et al., 2020). Consequently, predicted longshore sediment transport rates frequently suffer inaccuracies, relying solely on forecasts derived from limited data and empirical calibration constants.

This case report aims to provide direct hydrodynamic measurements from the upper shoreface of a sandy beach in Paraná. Furthermore, these data have the potential to enhance the comprehension of coastal processes and serve as valuable resources to validate

Submitted: 22-Jun.-2023
Approved: 06-Apr.-2024

Editor: Rubens Lopes

and calibrate numerical models and coastal engineering projects.

METHODS

The field experiment took place at Gaivotas Beach, Matinhos-PR, positioned at coordinates 25.725944° S and 48.482992° W, situated within the 34.5 km expanse of the Matinhos-Pontal do Sul beach arc (Figure 1). This sandy beach experiences semidiurnal microtidal conditions, with a spring tidal range of 1.5 m, and is exposed to a moderate-to-high energy storm wave climate. The transition to an intermediate-state rhythmic bar occurs due to an increase in grain size at this location (Borzone et al., 1996; Angulo et al., 2016). The beach spans approximately 60 m in width, characterized by a mean grain size of 1.89 Φ and intertidal slopes ranging from 1/30 to 1/25, along with high dimensionless fall velocity (Ω) values ranging from 2.9 to 2.5 (Borzone et al., 1996). The combination of south-southeast winds, elevated sea levels (storm surge), and large waves represents the most energetic events along the coastline, amplifying coastal currents (Noernberg and Alberti, 2014). Over one year of measurements at a depth of 18 m, the data showed a mean significant wave height of 1.6 m, with a maximum significant wave height of 4.8 m, a mean peak period of 8.4 s, and a maximum of 17.8 s (Angulo et al., 2016).

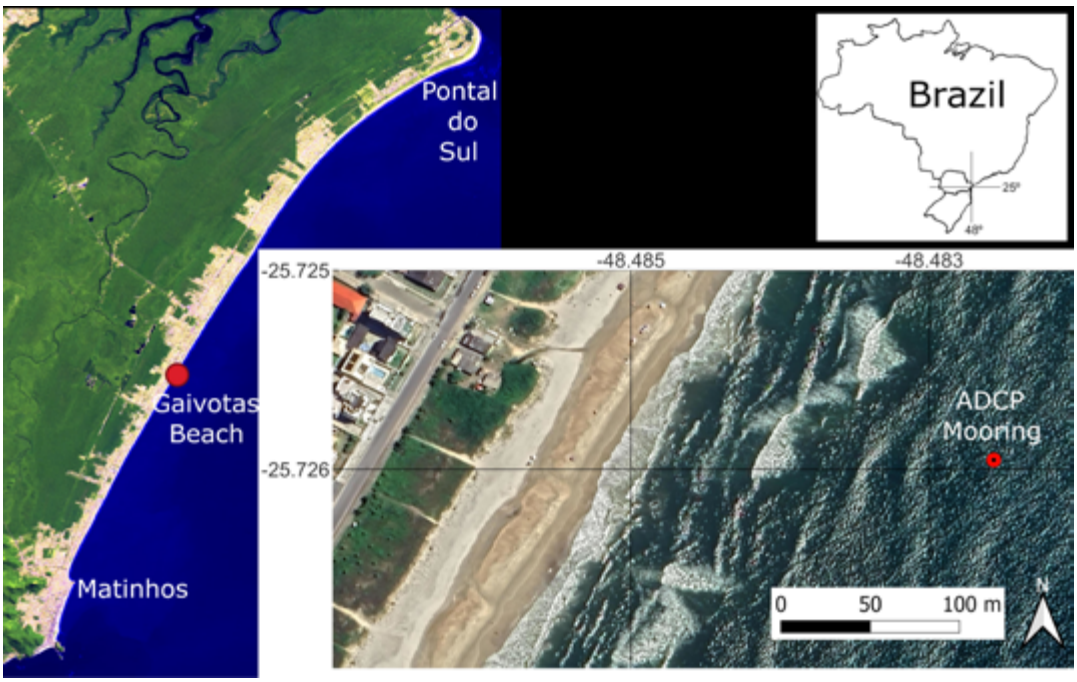

Figure 1. Study area with mooring position.

A time series of current velocity, significant wave height (Hs), peak period (Tp), and temperature were acquired behind the surf zone at the upper shoreface during the early austral autumn. The measurements were conducted with a moored instrument comprising a bottom-mounted acoustic Doppler current profiler (ADCP). Specifically, a 750 kHz ADCP SonTek/YSI Inc Argonaut XR model equipped with an integrated piezoresistive pressure sensor was deployed at an average depth of 5 m and approximately 200 m offshore. Depth-integrated current data were logged every 15 minutes, starting at a distance of 1.1 m from the sea bottom (0.8 m from the transducers). The moored instrument was operational from 12:00 AM on April 7th to 07:45 AM on April 28th, 2022, with all times reported in -3UTC. Detailed ADCP data can be found in the Supplementary Material.

Following the coastline orientation, moored current velocity vectors underwent a 30-degree rotation before being decomposed into alongshore (u) and cross-shore (v) components, where

positive *u* values indicate a northward direction and positive *v* values denote offshore movement. Wind data from a portable meteorological station (WS-2902) situated at Gaivotas Beach was provided by the Coastal Oceanography and Geoprocessing Laboratory of the Center for Marine Studies at the Federal University of Paraná.

The wave force (P), denoting the wave energy flux per unit crest length and expressed as kW m^{-1}, was computed (eq. 1) to delineate extreme events. This approach captures the synergy of high Hs and Tp values, indicative of the most intense wave energy events.

$$P = \frac{\rho g^2}{64\pi} Hs^2 Tp \qquad \text{eq. 1}$$

where ρ is the water density (1027 kg m^{-3}) and g is the acceleration due to gravity.

RESULTS AND DISCUSSION

The analysis of oceanographic variability during the mooring period reveals five distinct conditions (Figure 2). Initially, prevailing winds from the N-NE quadrant (Figure 2a) induce consistent southward longshore currents (Figure 2b). As the pre-frontal phase sets in around 04/09, wind directions oscillate between the SE and SW quadrants, resulting in a slight increase in Hs (Figure 2c) and occasional shifts in longshore currents influenced by tidal dynamics. By 04/14, the frontal system was fully established, characterized by strong S-SE winds peaking at 6 m s^{-1}. These winds initially drive a decrease in Tp followed by a subsequent rise (max. 15.7 s) (Figure 2d), accompanied by an increase in Hs (max. 2.52 m) and wave power (45.94 kW m^{-1}). During this condition, northward longshore currents dominate, reaching 73.28 cm s^{-1} (Table 1), with offshore flows hitting 30.58 cm s^{-1} (Figure 2e). This frontal system coincides with syzygy tide (Figure 2f), manifesting in sustained northward longshore intensity without inversion. Entering the post-frontal period around 04/19, the intensity of the wind diminishes, reverting to oscillations between the SE and SW quadrants. This condition shows a decline in wave height and longshore current intensity. Longshore currents exhibit oscillatory behavior, alternating between northward and southward flow, influenced by tidal effects, initially favoring northward flow until 04/21, then shifting to southward flow. Finally, after 04/25, prevailing winds revert to the NE quadrant, driving persistent southward longshore currents and occasionally showing minor tide-induced inversions during flood tides.

The relaxing of NE winds at the pre-frontal condition onset led to a rapid rise of 1.54 °C in seawater temperature within 3.5 hours, followed by a subsequent decline during the frontal event (Figure 2g). Abrupt temperature changes have been previously documented in the region, characterized by seasonal warming and cooling in coastal waters occurring discretely rather than continuously (Paloschi and Noernberg, 2021). The passage of cold fronts acts like pulses, amplifying mixing and advective processes (Noernberg and Alberti, 2014, Paloschi and Noernberg, 2021).

Table 1. Range in coastal currents properties obtained from June 19th–July 28th, 2019, mooring at upper shoreface in Gaivotas Beach. V is current velocity; *u* is alongshore current; *v* is cross-shore current; Hs is significant wave height; Tp is peak period, and P is wave force.

Variable	Min - Max	Mean ± SD
Temperature (°C)	23.17 - 26.08	24.34 ± 0.65
V (cm s^{-1})	74.63 (max)	14.28 ± 12.16
u northward (cm s^{-1})	73.28 (max)	16.20 ± 14.23
u southward (cm s^{-1})	49.67 (max)	9.69 ± 8.50
v offshore (cm s^{-1})	30.58 (max)	4.15 ± 3.91
v onshore (cm s^{-1})	14.05 (max)	2.53 ± 2.31
Hs (m)	2.52 (max)	0.90 ± 0.46
Tp (s)	2.4 - 18.1	9.60 ± 2.55
P (kW m^{-1})	45.94 (max)	5.19 ± 6.06

The predominantly northward longshore currents in the region have been extensively documented (Noernberg and Alberti, 2014; Angulo et al., 2016; Trombetta et al., 2020). Waves from the ESE and SE, generally associated with frontal systems, generate northward longshore currents and waves from N-NE result in southward longshore currents (Noernberg and Alberti, 2014; Oliveira et al., 2019). Although wave direction data were not obtained in this study, measurements in the upper shoreface provide additional insights into the relative significance of longshore and cross-shore flow.

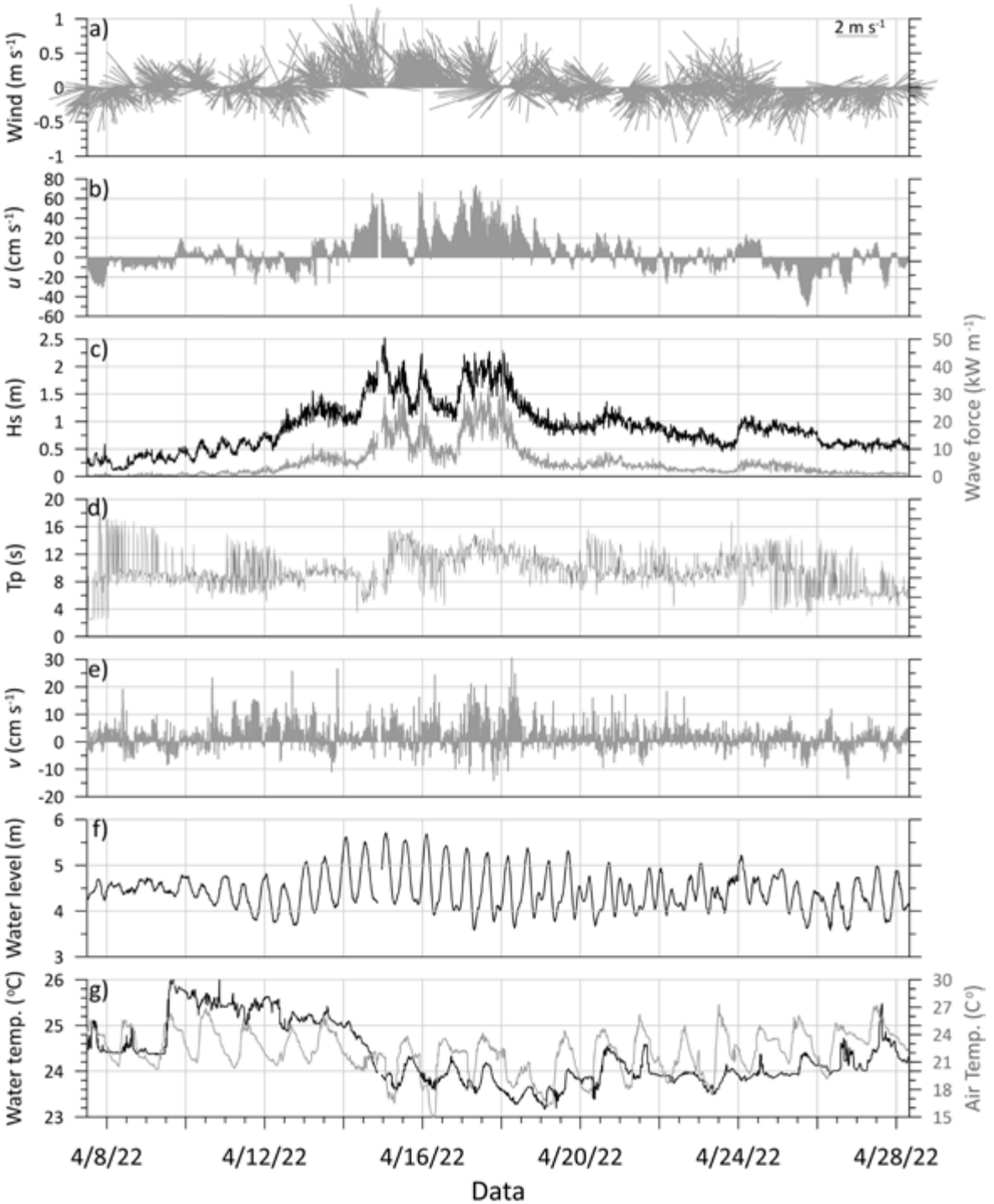

Figure 2. Time series of moored ADCP at the upper shoreface in Gaivotas Beach (April 07th–April 28th, 2022). (a) wind velocity; (b) depth-averaged alongshore flow (*u*) (positive values indicate northward flows and negative values, southward); (c) significant wave height (black line) and wave force (gray line); (d) wave peak period; (e) depth-averaged cross-shore flow (*v*) (positive values indicate offshore flows and negative values onshore), (f) water level above the bottom; and (g) near-bottom temperature (black line) and air temperature (gray line).

Wave height showed a notable positive correlation with northward longshore currents (Figure 3a), whereas southward flow was more intense when Hs ranged from 0.5 to 1 meter. In contrast, cross-shore currents showed no clear pattern in relation to wave height (Figure 3b). The tide exerted a minor influence on longshore currents compared to wave height (Figure 3c). However, the tide still played a discernible role, particularly in intensifying southward flows during low tide. The cross-shore currents were more pronounced during offshore and onshore low tides, being more intense offshore (Figure 3d).

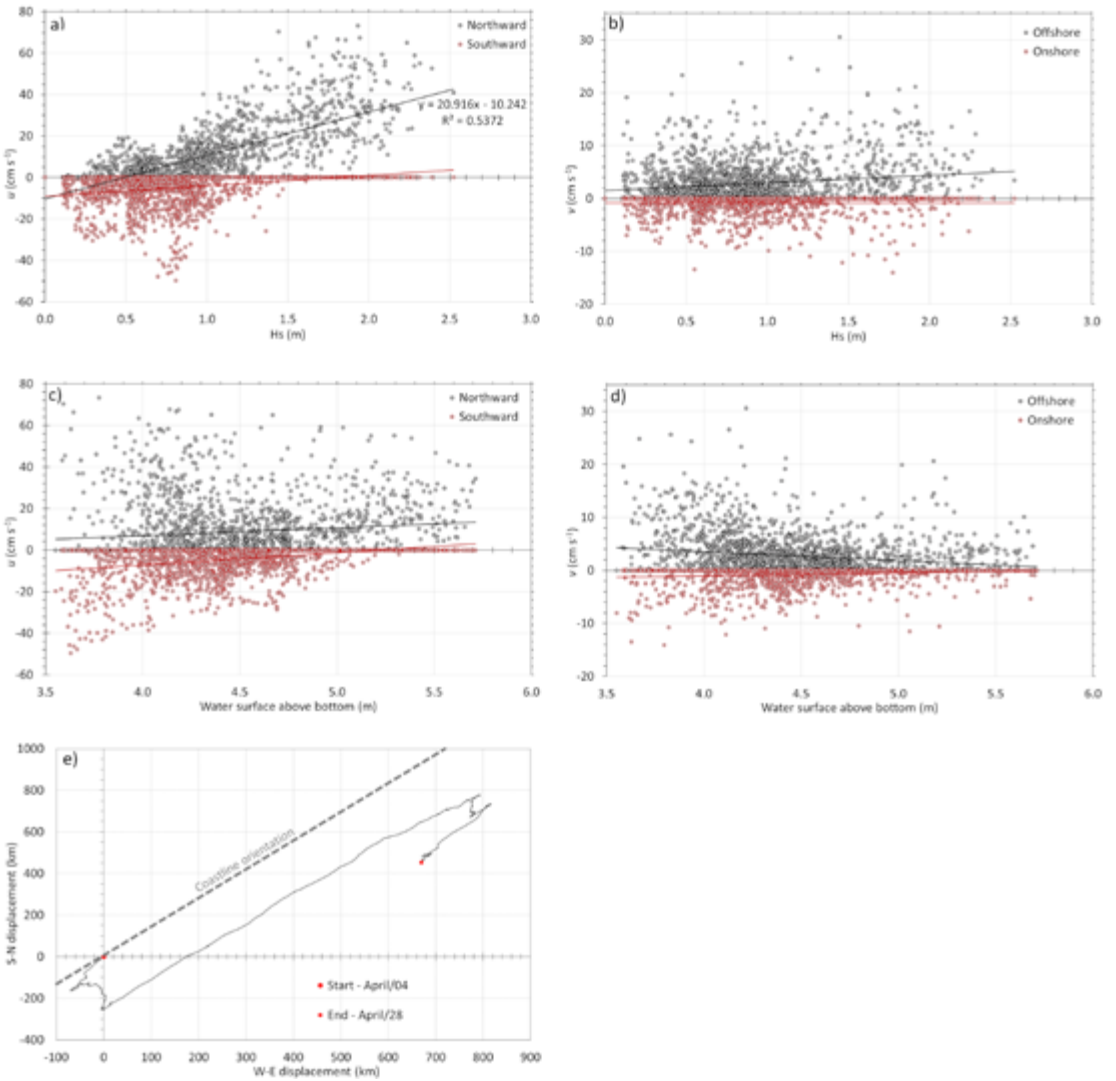

Figure 3. a) Relationship between Hs and longshore currents; b) relationship between Hs and cross-shore currents; c) relationship between tide (water surface above bottom) and longshore currents; d) relationship between tide (water surface above bottom) and cross-shore currents; and e) progressive vector diagram. For cross-shore currents, black circles are offshore and red onshore. For longshore currents, black circles are northward and red southward.

To evaluate the displacement by the longshore and crossshore flows, we analyzed the progressive vector. It is an estimate of the displacement of a particle resulting from the velocity measured in each time interval starting at the mooring position. The beginning of the displacement corresponds to the subsequent measurement and the end of the previous displacement. Although considering the flow speed in different locations is the same as the measurement location (mooring), it is a helpful representation for evaluating particle displacement.

During the pre- and post-frontal periods, when tidal oscillations exert more influence on flow direction, cross-shore flow surpasses longshore flow with a prevailing offshore direction. In the pre-frontal period, seaward displacement covered approximately 80 km over four days along the coastline. During relatively calm sea states with N-NE winds, southward longshore currents were predominant. Conversely, higher energy conditions, characterized by S-SE winds, led to the dominance of northward longshore currents. Notably, the northward advection during the high-energy event spanned approximately 900 km over eight days (Figure 3e).

Despite the relatively brief duration of the experiment, we capture significant variability in the magnitude and frequency of coastal processes and their driving forces. Whereas wave forces directly influence longshore currents, the nonlinear relationship between these variables results in substantial fluctuations in signal frequency across daily, fortnightly, sub-seasonal, seasonal, and interannual timescales (Silva et al., 2012).

CONCLUSION

Accurate assessments of shoreline changes are imperative for successful spatial planning, coastal engineering endeavors, sustainable coastal development, and climate change mitigation efforts along coastlines. In this study, we provided precise hydrodynamic data from the upper shoreface, situated just beyond the surf zone, in which complex interactions between waves, wind, and tidal currents occur. We also characterized the variability of longshore and cross-shore currents during a high-energy frontal event. This dataset is invaluable for researchers who quantify and model longshore sediment transport and morphological changes.

ACKNOWLEDGMENTS

The authors wish to honor the memory and legacy of Paulo da Cunha Lana, a remarkable professor, supportive friend, insightful scientist, and passionate mentor. His influence and guidance have left an indelible mark on the careers and analytical skills of countless students and professionals studying worms, mangroves, estuaries, coastal communities, and oceans worldwide. They also thank the anonymous reviewers for their valuable comments, which improved the manuscript.

AUTHOR CONTRIBUTIONS

M.A.N.: Conceptualization; Investigation; Visualization; Writing – original draft.

P.A.R.: Investigation; Visualization; Writing – original draft.

REFERENCES

Angulo, R. J., Borzone, C. A., Noernberg, M. A., Quadros, C. J. L., Souza, M. C. & Rosa, L. C. 2016. The State of Paraná Beaches. *In:* Short, A. D.; Klein, A. H. F. (Ed.). *Brazilian Beach Systems*. Coastal Research Library (pp. 419-464). Dordrecht: Springer.

Borzone, C. A., Souza, J. R. B. & Soares, A. G. 1996. Morphodynamic influence on the structure of inter and subtidal macrofaunal communities of subtropical sandy beaches. *Revista Chilena de Historia Natural*, 69, 565–577.

Hamon-Kerivel, K., Cooper, A., Jackson, D., Sedrati, M. & Pintado, E. G. 2020. Shoreface mesoscale morphodynamics: A review. *Earth-Science Reviews*, 209, 103330. DOI: https://doi.org/10.1016/j.earscirev.2020.103330

Hinkel, J., Nicholls, R. J., Tol, R. S. J., Wang, Z. B., Hamilton, J. M., Boot G., Vafeidis, A. T., Mcfadden L., Ganopolski, A. & Klein, R. J. T. 2013. A global analysis of erosion of sandy beaches and sea-level rise: An application of DIVA. *Global and Planetary Change*,111,150–158. DOI: https://doi.org/10.1016/j.gloplacha.2013.09.002

Luijendijk, A., Hagenaars, G., Ranasinghe, R., Baart F., Donchyts G. & Aarninkhof, S. 2018. The State of the World's Beaches. *Scientific Reports*, 8, 6641. DOI: https://doi.org/10.1038/s41598-018-24630-6

Noernberg, M. & Alberti, A. 2014. Oceanographic variability in the inner shelf of Paraná, Brazil: Spring condition. *Revista Brasileira de Geofísica*, 32, 197–206. DOI: dx.doi.org/10.22564/rbgf.v32i2.451

Oliveira, B. A., Sobral, F., Fetter, A. & Mendez, F. J. 2019. A high-resolution wave hindcast off Santa Catarina (Brazil) for identifying wave climate variability. *Regional Studies in Marine Science*, 32, 100834. DOI: dx.doi.org/10.1016/j.rsma.2019.100834

Paloschi, N. G. & Noernberg, M. A. 2021. Satellite products performance based on in-situ data to evaluate SST variability in a subtropical inner shelf in Brazil. Continental Shelf Research, 228, 104553. DOI: https://doi.org/10.1016/j.rsma.2019.100834

Silva, A. N., Taborda, R., Bertin, X. & Dodet, G. 2012. Seasonal to decadal variability of longshore sand transport at the northwest coast of Portugal. *Journal of Waterway, Port, Coastal, and Ocean Engineering*, 138(6), 464–472. DOI: dx.doi.org/10.1061/(ASCE)WW.1943-5460.0000152

Trombetta, T. B., Marques, W. C., Guimarães, R. C. & Costi, J. 2020. An overview of longshore sediment transport on the Brazilian coast. *Regional Studies in Marine Science*, 35, 101099. DOI: dx.doi.org/10.1016/j.rsma.2020.101099